
ProWAFt: A ROMA-LPD Instance for Workload-Aware and Dynamic Fault Tolerance in FPGA-Based CNN Accelerators

Xinxin Chen

Department of Computer Science
University of Chinese Academy of Sciences

Haoran Qiao

Department of Computer Science
University of Chinese Academy of Sciences

Yiming Guo

Department of Computer Science
University of Chinese Academy of Sciences

Kecheng Luo

Department of Computer Science
University of Chinese Academy of Sciences

Siyuan Feng

Department of Computer Science
University of Chinese Academy of Sciences

Jingwen Ma

Department of Computer Science
University of Chinese Academy of Sciences

Abstract

SRAM-based FPGAs provide an attractive platform for energy- and latency-constrained CNN inference at the network edge, yet transient faults can lead to silent errors that compromise reliability. Always-on redundancy (e.g., full TMR) improves correctness but incurs substantial performance and energy overhead, while reactive recovery may introduce unacceptable latency on the critical path. We propose **ProWAFt**, a proactive workload-aware fault-tolerance framework for FPGA-based CNN accelerators that uses partial reconfiguration to selectively apply TMR across reconfigurable partitions. ProWAFt quantifies workload criticality, models fault propagation and reconfiguration overhead, and selects configurations that minimize a composite objective over latency, energy, and reliability risk. Implemented on a Xilinx Zynq UltraScale+ ZCU104 platform with six reconfigurable regions and evaluated on a 500-task trace derived from ResNet-18, MobileNetV2, and EfficientNet-Lite under time-varying SEU injection, ProWAFt achieves lower composite cost than static TMR and reactive reconfiguration while maintaining high task success rate and near-baseline throughput with low online decision overhead.

1 Introduction

Convolutional neural networks (CNNs) are now routinely deployed on edge platforms for perception and monitoring tasks where latency and energy are tightly constrained. FPGA-based accelerators are a practical option in this regime: they offer domain-specific parallelism while retaining post-deployment flexibility through reconfiguration. As deployments scale and move into harsher operating environments, however, reliability becomes a limiting factor rather than a secondary concern. Shanghai AI Lab et al. [2025]

SRAM-based FPGAs are vulnerable to transient disturbances that can corrupt configuration bits or on-chip computation, leading to silent errors in CNN inference. The difficulty is that fault impact is highly non-uniform. Both the fault risk (e.g., varying with time and operating conditions) and the workload sensitivity (e.g., layer type, precision, and error-propagation behavior) can change substantially across an execution trace. Figure 1 summarizes the resulting mismatch: a fixed protection level assumes a

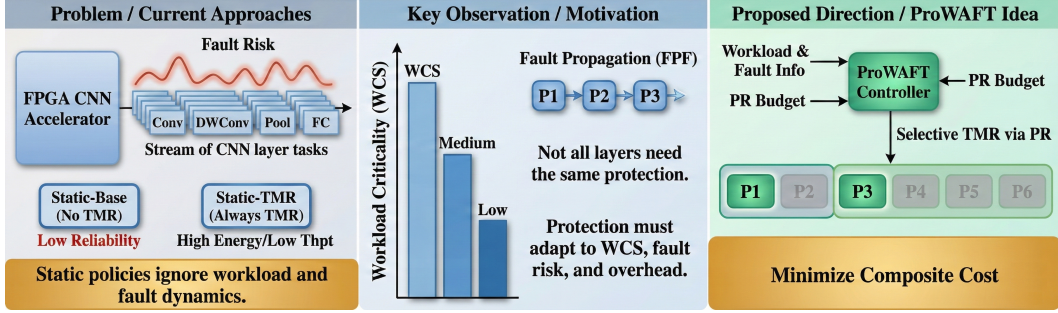


Figure 1: Motivation for ProWAFt. Static approaches fail by ignoring dynamic fault risks and varied workload criticality. ProWAFt addresses this by proactively adapting protection based on Workload Criticality (WCS), real-time fault risk, and reconfiguration overhead. The controller manages selective TMR via Partial Reconfiguration (PR) to balance performance, energy, and reliability, minimizing composite cost.

stationary environment and a homogeneous workload, neither of which holds in practice. Wen et al. [2026]

A common mitigation is to apply triple modular redundancy (TMR) statically, which improves robustness but also increases resource usage and power, and can reduce throughput on constrained devices. At the other extreme, running without redundancy preserves efficiency but exposes the system to unacceptable error rates when fault risk increases. Reactive recovery schemes that reconfigure only after detecting a fault reduce steady-state overhead, but they pay the cost on the critical path and can violate latency constraints. These trade-offs indicate that reliability should be treated as a runtime decision rather than a one-time design choice. Gao et al. [2025]

This work presents **ProWAFt**, a proactive workload-aware fault-tolerance framework for FPGA-based CNN accelerators. ProWAFt uses runtime telemetry (workload features and estimated per-partition fault probabilities) together with offline-characterized partial reconfiguration (PR) overhead to decide when and where to enable protection. The approach quantifies workload criticality, models fault propagation and recovery risk across reconfigurable partitions, and selects a configuration that minimizes a composite objective spanning performance, energy, and reliability while accounting for PR cost. In our implementation on a Zynq UltraScale+ ZCU104 platform with six reconfigurable regions and a 500-task CNN workload trace, ProWAFt reduces composite cost relative to static and reactive baselines while keeping decision overhead small. Li et al. [2025]

Contributions.

- We formulate proactive, workload-aware fault tolerance for FPGA-based CNN accelerators as a runtime configuration problem that enables *selective TMR* via partial reconfiguration, explicitly trading off latency, energy, and reliability under reconfiguration constraints.
- We introduce a lightweight modeling stack for decision-making, including a *Workload Criticality Score (WCS)* and a fault-propagation-based risk formulation (FPF/RRS), and integrate these components into a composite cost used for configuration selection.
- We implement ProWAFt on a ZCU104 platform and evaluate it under a time-varying SEU injection model using diverse CNN-layer workloads. Results show improved composite cost and adaptive protection behavior, with low online decision overhead and quantified PR costs.

2 Related Work

2.1 FPGA Soft Errors

SRAM-based FPGAs are susceptible to transient faults such as single-event upsets (SEUs), which may corrupt configuration bits and lead to silent malfunctions. Prior work has explored mitigation

across the stack, including configuration scrubbing (periodic or adaptive), protection of state with ECC/parity, and hardware redundancy such as TMR/DWC . These techniques can substantially improve reliability, but their overhead is non-trivial and often workload- and platform-dependent. In edge inference, where power and latency margins are limited, always-on redundancy is frequently too expensive, while purely reactive recovery can incur unacceptable latency spikes. Tang et al. [2022c]

2.2 CNN Reliability

A growing body of work studies the reliability of CNN/DNN inference under faults via fault injection, statistical error models, and vulnerability analysis. A consistent observation is that fault impact is not uniform: different layer types, precisions, and activation behaviors exhibit different sensitivities, and errors may amplify as they propagate through the network. This has motivated selective protection and lightweight detection strategies for DNN accelerators. However, many existing approaches either assume a fixed protection plan chosen offline or do not explicitly model how faults propagate through dependent accelerator stages in a partitioned design. Liu et al. [2023]

2.3 Partial Reconfiguration

Partial reconfiguration (PR) has been widely used to time-multiplex accelerator functions, specialize datapaths to changing models, and adapt resource allocation at runtime. PR also enables adaptive reliability by switching between baseline and hardened variants (e.g., TMR-protected modules) when conditions warrant . Existing PR-based fault-tolerance schemes are often reactive (triggered after an error) or rely on fixed thresholds, and they may not explicitly account for the time/energy overhead of PR in the decision objective. This can lead to protection being applied too late, too broadly, or too frequently. Tang et al. [2022a]

2.4 Runtime Policies

Runtime management under competing objectives (latency, energy, and reliability) has been addressed using rule-based switching, heuristic controllers, and optimization/learning-based policies such as MDP or RL formulations. These methods demonstrate the value of formal decision-making, but they typically adopt coarse reliability surrogates and do not incorporate workload-dependent fault criticality together with fault propagation and PR overhead in a unified cost model. ProWAFt differs by combining workload criticality scoring with propagation-aware risk modeling and an explicit PR cost term, enabling proactive selective TMR decisions that track both workload variation and time-varying fault risk. Feng et al. [2024]

3 Methodology: Proactive Workload-Aware Fault Tolerance (ProWAFt) for CNN Accelerators

This section presents **ProWAFt**, a runtime framework that enables workload-adaptive fault tolerance for FPGA-based CNN accelerators via Partial Reconfiguration (PR). ProWAFt decides *when* and *where* to enable protection (e.g., TMR variants) by jointly considering (i) workload characteristics, (ii) estimated partition-level fault risk, and (iii) PR overhead (Fig. 2).

3.1 System Model and Problem Formulation

We model the accelerator as a set of K reconfigurable partitions $\mathcal{P} = \{P_1, \dots, P_K\}$. Each partition P_k can be configured with one of N_k pre-synthesized hardware functions from a library \mathcal{F}_k . In our setting, \mathcal{F}_k includes both baseline and protected (e.g., TMR) variants for supported kernels. A **system configuration** is denoted by $C_j \in \mathcal{C}$. Zhao et al. [2024a] Zhao et al. [2024b]

The accelerator processes a stream of workloads $\mathcal{W} = \{W_1, W_2, \dots\}$, where each W_i corresponds to a CNN layer (or a small group of layers) described by a feature vector \mathbf{v}_i (e.g., operator type, input shape, precision, batch size). We denote by $\mathcal{C}(W_i) \subseteq \mathcal{C}$ the set of **feasible configurations** for workload W_i , i.e., configurations that implement the required kernels and precision for W_i . Wang et al. [2025a] Tang et al. [2023]

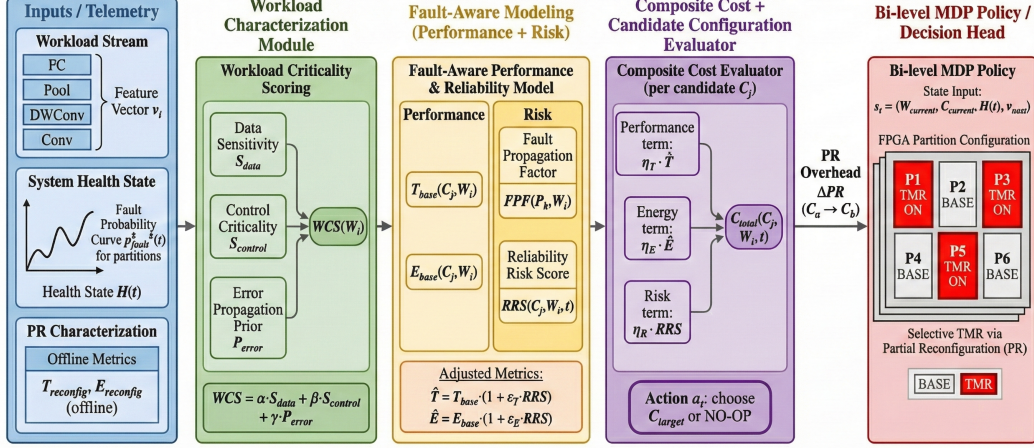


Figure 2: Architectural overview of the ProWAFt pipeline. Input telemetry from workloads and system health is processed sequentially through four stages: (1) Workload Criticality Scoring (WCS); (2) Fault-Aware Performance & Risk Modeling; (3) Composite Cost Evaluation based on weighted metrics and PR overhead; and finally, (4) a Bi-level MDP Policy that determines the optimal proactive selective TMR action for the FPGA partitions.

The system health state at time t is represented by $\mathbf{H}(t) = \{p_1^{fault}(t), \dots, p_K^{fault}(t)\}$, where $p_k^{fault}(t)$ is the estimated transient fault probability for partition P_k . PR is performed between workloads and incurs time/energy overhead; we model a constrained reconfiguration budget B_{PR} (time and/or energy) over an execution window. Sun et al. [2025] Lu et al. [2024]

Objective. For each incoming workload W_i , given the current configuration $C_{current}$, health state $\mathbf{H}(t)$, and remaining budget B_{PR} , ProWAFt selects an action (reconfigure to some $C_j \in \mathcal{C}(W_i)$ or stay) to minimize an expected composite cost that captures latency, energy, and reliability risk while accounting for PR overhead. Zhao et al. [2025] Tang et al. [2024b] Tang et al. [2024a]

3.2 Workload Characterization and Criticality Scoring

We define a **Workload Criticality Score (WCS)** to quantify how sensitive W_i is to hardware faults:

$$WCS(W_i) = \alpha \cdot S_{data}(W_i) + \beta \cdot S_{control}(W_i) + \gamma \cdot P_{error}(W_i), \quad (1)$$

where $\alpha + \beta + \gamma = 1$ and each term is normalized to $[0, 1]$. Shan et al. [2024] Feng et al. [2023] Tang et al. [2022b]

- $S_{data}(W_i)$ (**data sensitivity**) is derived from the entropy of the output activation distribution. In practice, we estimate it using offline profiling on a calibration set and store layer-wise statistics as a lookup table indexed by operator type/shape/precision.
- $S_{control}(W_i)$ (**control criticality**) flags workloads on conditional paths (0/1). For standard feed-forward CNNs without dynamic control flow, this term is set to 0.
- $P_{error}(W_i)$ (**error propagation likelihood**) is obtained from lightweight pre-characterization (e.g., single-bit fault injection) and stored as a compact table or regression model. It approximates the probability that a fault in the current workload causes a task-level critical error at the output.

3.3 Fault-Aware Performance and Reliability Modeling

For a candidate configuration $C_j \in \mathcal{C}(W_i)$, ProWAFt predicts fault-free performance/energy, and then estimates reliability risk under $\mathbf{H}(t)$.

1) Baseline (fault-free) metrics.

$$T_{base}(C_j, W_i) = \sum_{k=1}^K \frac{Ops_k(W_i)}{f_k \cdot PE_k(C_j)} + T_{comm}(C_j, W_i), \quad (2)$$

$$E_{base}(C_j, W_i) = \sum_{k=1}^K P_k^{dyn}(C_j) \cdot \frac{Ops_k(W_i)}{f_k \cdot PE_k(C_j)} + P_{static}(C_j) \cdot T_{base}(C_j, W_i). \quad (3)$$

Here $Ops_k(W_i)$ denotes the operations mapped to P_k for W_i , f_k is the clock frequency, $PE_k(C_j)$ is the number of active processing elements, $P_k^{dyn}(C_j)$ is dynamic power, and $P_{static}(C_j)$ is static power of the active configuration. Fu et al. [2024] Guo et al. [2025] Wang et al. [2025c]

2) Fault propagation and risk. We define a **Fault Propagation Factor (FPF)** for each partition:

$$FPF(P_k, W_i, C_j) = WCS(W_i) \cdot \lambda_k(C_j) \cdot Fanout(P_k, C_j), \quad (4)$$

where $\lambda_k(C_j) \in [0, 1]$ is the utilization ratio of P_k under C_j , and $Fanout(P_k, C_j)$ is the number of downstream partitions that consume P_k 's outputs in the datapath induced by C_j . Wang et al. [2025b] Feng et al. [2025] Lu et al. [2025] Fei et al. [2025] We then compute a **dimensionless Reliability Risk Score**:

$$RRS(C_j, W_i, t) = \frac{1}{Z} \sum_{k=1}^K p_k^{fault}(t) \cdot FPF(P_k, W_i, C_j) \cdot \rho_k, \quad (5)$$

where $\rho_k \in [0, 1]$ is a normalized severity weight reflecting how costly a fault in P_k is (e.g., based on recovery difficulty or observed output impact), and Z is a normalization constant chosen so that $RRS \in [0, 1]$ over the considered candidate set.

To couple risk with efficiency metrics, we use fault-aware predictions:

$$\hat{T} = T_{base} \cdot (1 + \epsilon_T \cdot RRS), \quad \hat{E} = E_{base} \cdot (1 + \epsilon_E \cdot RRS),$$

where ϵ_T and ϵ_E are obtained from offline fault characterization.

3) PR overhead. Switching from C_a to C_b incurs:

$$\Delta_{PR}(C_a \rightarrow C_b) = \omega_T \cdot T_{reconfig}(C_a, C_b) + \omega_E \cdot E_{reconfig}(C_a, C_b), \quad (6)$$

with $T_{reconfig}$ and $E_{reconfig}$ characterized offline.

3.4 Policy and Online Decision Rule

ProWAFt can be viewed as a sequential decision problem: at each step, the controller selects a reconfiguration action based on $(W_i, C_{current}, \mathbf{H}(t))$ and the remaining budget. We define the per-workload composite cost for a candidate configuration C_j as:

$$\mathcal{C}_{total}(C_j, W_i, t) = \eta_T \cdot \tilde{T}(C_j, W_i, t) + \eta_E \cdot \tilde{E}(C_j, W_i, t) + \eta_R \cdot RRS(C_j, W_i, t), \quad (7)$$

where η_T, η_E, η_R are application weights and \tilde{T}, \tilde{E} are normalized latency/energy terms (e.g., normalized to the fault-free static-base reference for the same workload) to keep the objective dimensionless and comparable across workloads.

In our implementation, we use a low-overhead receding-horizon controller: for each incoming W_i , we evaluate a finite candidate set $\mathcal{C}(W_i)$ (or a pruned subset) and choose the configuration that minimizes the immediate objective plus PR overhead, subject to the remaining budget:

$$J(C_j) = \mathcal{C}_{total}(C_j, W_i, t) + \mathbb{I}[C_j \neq C_{current}] \cdot \Delta_{PR}(C_{current} \rightarrow C_j). \quad (8)$$

The selected action is $a_t = \arg \min_{C_j \in \mathcal{C}(W_i)} J(C_j)$, with infeasible actions filtered out when Δ_{PR} violates the current budget.

4 Experiments and Evaluation

This section evaluates **ProWAFt** on a real FPGA platform under a controlled, time-varying fault injection setting. We answer four research questions: (1) **Effectiveness**: Does ProWAFt improve

the overall performance–energy–reliability trade-off compared to static and reactive baselines? (2) **Adaptivity**: Does ProWAFT adapt protection decisions to workload criticality and fault risk? (3) **Overhead**: What is the runtime overhead of decision-making and PR, and how does it compare to reactive recovery? (4) **Component contribution**: How much does each ProWAFT component contribute?

Unless otherwise stated, all methods are evaluated on the same 500-task trace and the same fault injection schedule (fixed random seed) for fair comparison.

4.1 Experimental Setup

4.1.1 Platform

We implement ProWAFT on a Xilinx Zynq UltraScale+ ZCU104 platform. The FPGA fabric is partitioned into $K=6$ reconfigurable regions. Each region can host one of the pre-synthesized accelerator variants (baseline and TMR-protected). Table 1 summarizes the platform and accelerator library.

Table 1: Experimental Platform Specifications and Accelerator Library

Component	Specification
FPGA Platform	Xilinx Zynq UltraScale+ ZCU104
Processor	ARM Cortex-A53 Quad-core @ 1.5GHz
FPGA Fabric	Kintex UltraScale+ (504K Logic Cells)
Reconfigurable Partitions (K)	6
Accelerator Library (\mathcal{F}_k)	
8-bit INT Convolution Engine (CE)	Baseline convolution accelerator
Max-Pooling Unit (PU)	Pooling operation accelerator
BatchNorm-Activation Unit (BAU)	BatchNorm and activation accelerator
CE-TMR / PU-TMR / BAU-TMR	TMR-protected versions (triplicated logic)

4.1.2 Workload trace

We construct a workload trace \mathcal{W} with 500 tasks derived from representative CNNs (ResNet-18, MobileNetV2, and EfficientNet-Lite). Each task corresponds to a supported layer type (Conv2D, DepthwiseConv2D, Pooling, FC) with varying input dimensions. Table 2 summarizes the trace.

Table 2: Workload Trace Characteristics

Parameter	Value/Range
Total Workloads	500
CNN Models	ResNet-18, MobileNetV2, EfficientNet-Lite
Layer Types	Conv2D, DepthwiseConv2D, Pooling, FC
Input Dimensions	32×32 to 224×224
Workload Criticality (WCS) Range	0.15 – 0.85

4.1.3 Fault injection and detection

We inject transient faults as single-event upsets (SEUs) targeting configuration memory bits. The per-partition fault probability $p_k^{fault}(t)$ varies over time (sinusoidal component plus random baseline) within $[0.001, 0.01]$. Table 3 lists the fault model settings. Faults are detected using a lightweight parity check; upon detection, the reactive baseline triggers recovery by switching to protected configurations.

4.1.4 Metrics and baselines

We compare ProWAFT against three baselines: **Static-Base** (always baseline accelerators), **Static-TMR** (always TMR variants), and **Reactive-Reconfig (RR)** (reconfigure to TMR only after fault

Table 3: Fault Injection Model Parameters

Parameter	Value
Fault Type	Single-Event Upset (SEU)
Injection Target	Configuration memory bits
Fault Probability $p_k^{fault}(t)$ Range	0.001 – 0.01
Probability Variation	Sinusoidal + random baseline
Fault Detection Method	Lightweight parity check

detection). We report composite cost C_{total} (Eq. 7) as the primary metric, together with normalized throughput, system energy, task success rate, and PR overhead. Table 4 summarizes metrics and baselines. Unless otherwise specified, we use $(\eta_T, \eta_E, \eta_R) = (0.4, 0.3, 0.3)$.

Table 4: Evaluation Metrics and Baseline Methods

Category	Item	Description
Metrics	Composite Cost (C_{total})	Primary metric from Eq. 7
Metrics	Normalized Throughput	Workloads/sec, normalized to Static-Base
Metrics	System Energy (J)	Total energy consumed during the trace
Metrics	Task Success Rate (%)	Workloads completed without critical error
Metrics	Reconfiguration Overhead	Time/energy spent on PR events
Baselines	Static-TMR	All partitions use TMR-protected accelerators
Baselines	Static-Base	All partitions use baseline (non-TMR) accelerators
Baselines	Reactive-Reconfig (RR)	Reconfigure to TMR only after fault detection
Weights	(η_T, η_E, η_R)	0.4, 0.3, 0.3 (balanced profile)

4.1.5 Measurement methodology

We measure end-to-end execution time over the full trace on the ARM processor (PS) and compute normalized throughput as workloads/sec normalized to Static-Base. PR time is measured by timestamping the start/end of each PR event. System energy is obtained by integrating measured power over the trace duration using the same procedure across all methods. For success rate, a workload is counted as successful if it completes and its output passes the defined correctness check (golden-reference comparison or application-defined tolerance).

4.2 Results

4.2.1 Trace profile visualization

To illustrate the evaluation setting, Fig. 3 visualizes the time-varying fault risk and workload criticality over the 500-task trace (used in all experiments).

4.2.2 Overall effectiveness (RQ1)

Table 5 reports overall performance. Static-Base achieves the highest throughput but suffers the lowest success rate. Static-TMR achieves perfect success but pays a large throughput and energy penalty. RR improves success rate but still incurs substantial overhead.

ProWAFt achieves the best trade-off: compared to Static-TMR, it improves normalized throughput from 0.61 to 0.89 (+45.9%), reduces energy from 302.5 J to 210.7 J (-30.3%), and maintains a high success rate (98.8%, 1.2 percentage points lower than Static-TMR). Compared to RR, ProWAFt improves throughput by 18.7%, reduces energy by 17.1%, improves success rate by 2.4 percentage points, and reduces C_{total} from 0.78 to 0.54 (30.8% relative reduction).

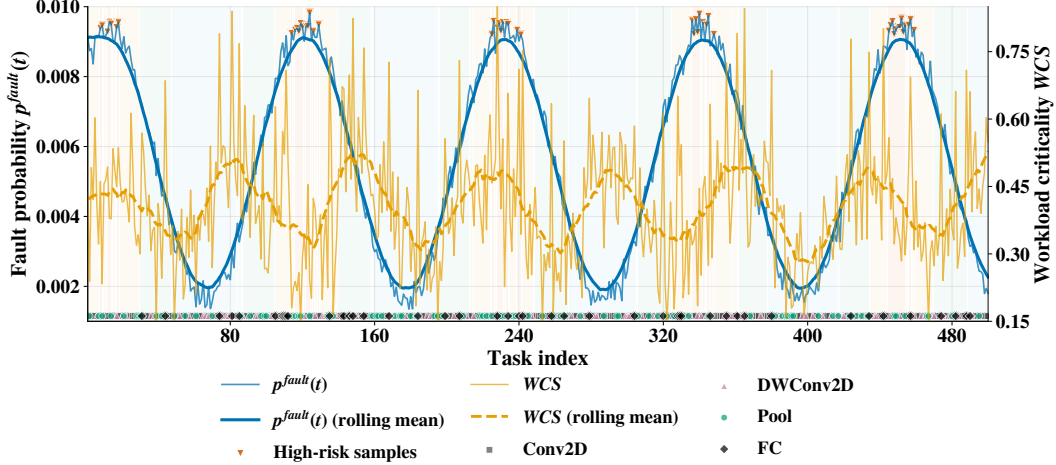


Figure 3: Workload trace and time-varying fault risk used in evaluation. Top: representative (or average) partition fault probability $p_k^{fault}(t)$ over the 500-task trace. Bottom: per-task workload criticality score (WCS).

Table 5: Overall Performance Comparison Across All Methods

Method	Norm. Throughput	Energy (J)	Success Rate (%)	C_{total}
Static-Base	1.00	185.2	78.0	0.72
Static-TMR	0.61	302.5	100.0	0.81
Reactive-Reconfig	0.75	254.1	96.4	0.78
ProWAFt (Ours)	0.89	210.7	98.8	0.54

We further visualize the operating points in Fig. 4, where ProWAFt lies in a favorable region compared to static and reactive baselines.

4.2.3 Adaptivity (RQ2)

Table 6 quantifies ProWAFt’s protection behavior across operational regimes. ProWAFt increases TMR usage as either fault risk or workload criticality rises, while maintaining stable sub-millisecond decision latency. Fig. 5 provides a timeline view of the adaptive decisions over the trace.

Table 6: ProWAFt Adaptation Behavior Across Operational Regimes

Operational Regime	Avg p^{fault}	Avg WCS	TMR Usage (%)	Avg Decision Latency (ms)
Low Risk	0.002	0.25	12.3	0.42
Moderate Risk	0.005	0.45	34.7	0.47
High Risk	0.009	0.70	78.9	0.51
Critical Workloads Only	0.003	0.80	95.2	0.38
Reactive-Reconfig Baseline	–	–	45.6	15.3 (post-fault)

4.2.4 Overhead (RQ3)

Table 7 breaks down decision and reconfiguration overhead. The total decision overhead is 0.50 ms (0.13 mJ), dominated by candidate evaluation and WCS computation. PR dominates proactive overhead. In the single-partition case, proactive overhead (decision+PR) is 4.70 ms, versus 15.30 ms for reactive recovery ($3.3\times$ lower). Even for multi-partition updates (9.00 ms), proactive overhead remains lower than reactive recovery. Zhang et al. [2026], Chen et al. [2025b,a], You et al. [2026], Zhao et al. [2026], Huang et al. [2026]

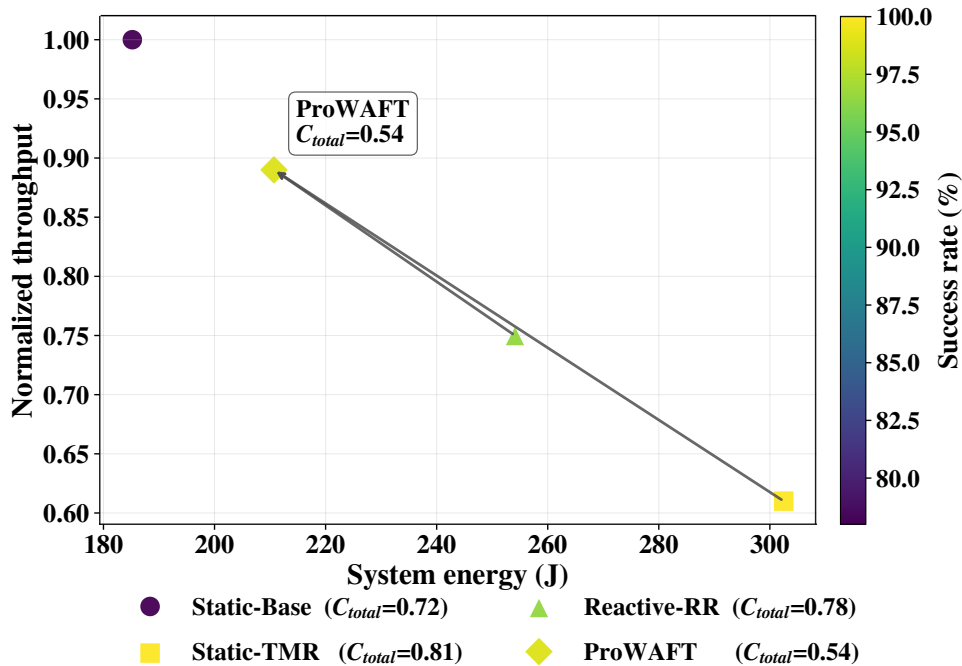


Figure 4: Energy–throughput trade-off with reliability annotation (e.g., point label or marker size indicates success rate). ProWAFt achieves a favorable operating point compared to static and reactive baselines.

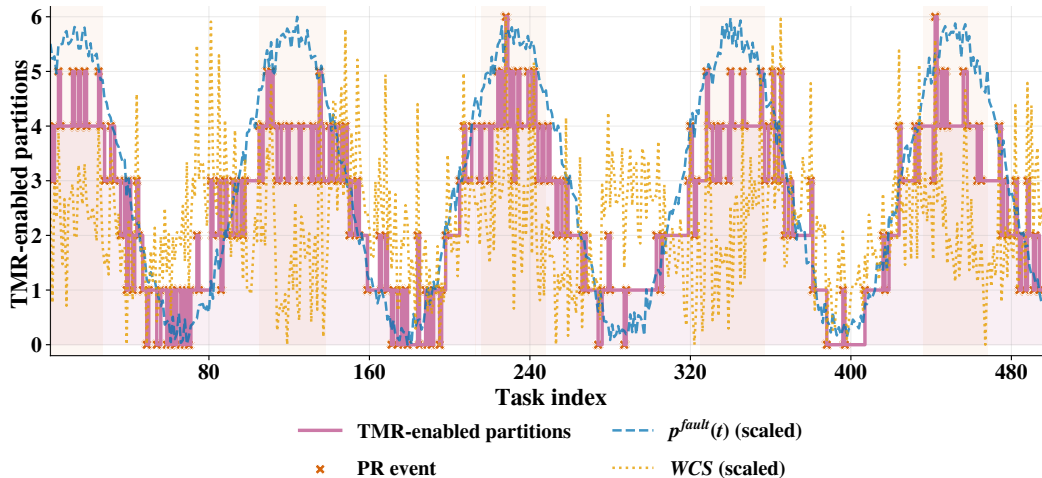


Figure 5: Adaptive protection behavior over time. Example visualization: number of TMR-enabled partitions (0–6) per task, with PR events marked. The reactive baseline typically responds after fault detection, while ProWAFt adjusts proactively.

4.2.5 Component contribution (RQ4)

Table 8 reports ablations. Removing WCS increases C_{total} and reduces success rate, showing that uniform criticality is insufficient. Removing the propagation model (FPF/RRS) reduces success rate (94.3%), despite similar throughput. Replacing the policy with a greedy strategy leads to the largest C_{total} increase (0.66).

Table 7: ProWAFt Decision and Reconfiguration Overhead Breakdown

Component	Time Cost	Energy Cost
Workload Feature Extraction	0.08 ms	0.02 mJ
WCS Computation (Eq. 1)	0.12 ms	0.03 mJ
Candidate Configuration Evaluation	0.25 ms	0.07 mJ
Policy Decision	0.05 ms	0.01 mJ
Total Decision Overhead	0.50 ms	0.13 mJ
Single Partition Reconfiguration	4.20 ms	1.10 mJ
Multi-Partition Reconfiguration (avg)	8.50 ms	2.25 mJ
Total Proactive Overhead (Decision+PR)	4.70–9.00 ms	1.23–2.38 mJ
Reactive Overhead (RR Baseline)	15.30 ms	4.05 mJ

Table 8: Ablation Study: Impact of Individual Components on System Performance

Method Variant	Norm. Throughput	Energy (J)	Success Rate (%)	C_{total}
Full ProWAFt	0.89	210.7	98.8	0.54
w/o WCS (uniform criticality)	0.85	228.3	95.1	0.63
w/o FPF (no propagation model)	0.88	215.4	94.3	0.61
w/o policy (greedy)	0.82	225.6	97.2	0.66
Degradation vs. Full	-7.9% to +8.3%	+2.2% to +8.3%	-4.6 to -1.6 pp	+13.0% to +22.2%

4.2.6 Sensitivity analysis

Table 9 studies sensitivity to objective weights and estimation errors. Shifting weights moves the operating point as expected, while moderate perturbations in WCS threshold and fault probability estimates cause limited degradation, indicating stable behavior under reasonable modeling errors.

Table 9: Sensitivity Analysis of ProWAFt to Key Parameters

Parameter Variation	C_{total}	Success Rate (%)	Reconfig. Events
Baseline ($\eta_T=0.4, \eta_E=0.3, \eta_R=0.3$)	0.54	98.8	127
Performance-focused ($\eta_T=0.6, \eta_E=0.3, \eta_R=0.1$)	0.48	96.2	89
Energy-focused ($\eta_T=0.3, \eta_E=0.6, \eta_R=0.1$)	0.52	96.8	103
Reliability-focused ($\eta_T=0.2, \eta_E=0.2, \eta_R=0.6$)	0.58	99.5	156
WCS Threshold +20%	0.57	97.1	112
WCS Threshold -20%	0.55	99.2	143
Fault Probability Estimate +25%	0.56	99.1	138
Fault Probability Estimate -25%	0.58	97.9	115

4.3 Summary of findings

Table 10 summarizes the answers to the four research questions.

5 Limitations

Our experiments employ software-based fault injection, which enables controlled evaluation but cannot capture all physical mechanisms. Future work will include radiation testing and thermal-stress testing, and will reduce reliance on offline characterization by enabling in-field self-calibration.

Table 10: Summary of Experimental Findings for Each Research Question

RQ	Key Finding	Supporting Evidence
Q1: Effectiveness	ProWAFt achieves the best overall trade-off, reducing C_{total} by 33.3% vs. Static-TMR and 30.8% vs. RR.	Table 5.
Q2: Adaptivity	ProWAFt adjusts TMR usage from 12.3% to 95.2% based on WCS and p^{fault} .	Table 6, Fig. 5.
Q3: Overhead	Online decision overhead is 0.50 ms; proactive (decision+PR) overhead is lower than reactive recovery.	Table 7.
Q4: Contribution	WCS , propagation modeling, and policy are all necessary; removing any increases C_{total} by 13–22%.	Table 8.

6 Conclusion

This paper presented **ProWAFt**, a proactive and workload-aware fault-tolerance framework for FPGA-based CNN accelerators. ProWAFt leverages partial reconfiguration to selectively enable TMR based on workload criticality and time-varying fault risk, while explicitly accounting for reconfiguration overhead in the decision objective. Experiments on a Zynq UltraScale+ ZCU104 platform with six reconfigurable partitions and a 500-task CNN-layer trace show that ProWAFt achieves a better overall performance–energy–reliability trade-off than static redundancy and reactive recovery, with sub-millisecond online decision overhead. Future work will validate the approach under physical fault campaigns (e.g., radiation/thermal stress) and extend the framework to larger accelerator libraries and longer-running deployments.

References

- Huiyi Chen, Jiawei Peng, Dehai Min, Changchang Sun, Kaijie Chen, Yan Yan, Xu Yang, and Lu Cheng. Mvi-bench: A comprehensive benchmark for evaluating robustness to misleading visual inputs in lvlms. In *Proceedings of the 43rd International Conference on Machine Learning (ICML 2026)*, 2025a.
- Kaijie Chen, Zihao Lin, Zhiyang Xu, Ying Shen, Yuguang Yao, Joy Rimchala, Jiaxin Zhang, and Lifu Huang. R2i-bench: Benchmarking reasoning-driven text-to-image generation. In *Proceedings of the 2025 Conference on Empirical Methods in Natural Language Processing*, pages 12606–12641, 2025b.
- Xiang Fei, Jinghui Lu, Qi Sun, Hao Feng, Yanjie Wang, Wei Shi, An-Lan Wang, Jingqun Tang, and Can Huang. Advancing sequential numerical prediction in autoregressive models. *arXiv preprint arXiv:2505.13077*, 2025.
- Hao Feng, Zijian Wang, Jingqun Tang, Jinghui Lu, Wengang Zhou, Houqiang Li, and Can Huang. Unidoc: A universal large multimodal model for simultaneous text detection, recognition, spotting and understanding. *arXiv preprint arXiv:2308.11592*, 2023.
- Hao Feng, Qi Liu, Hao Liu, Jingqun Tang, Wengang Zhou, Houqiang Li, and Can Huang. Docpedia: Unleashing the power of large multimodal model in the frequency domain for versatile document understanding. *Science China Information Sciences*, 67(12):1–14, 2024.
- Hao Feng, Shu Wei, Xiang Fei, Wei Shi, Yingdong Han, Lei Liao, Jinghui Lu, Binghong Wu, Qi Liu, Chunhui Lin, et al. Dolphin: Document image parsing via heterogeneous anchor prompting. *arXiv preprint arXiv:2505.14059*, 2025.
- Ling Fu, Biao Yang, Zhebin Kuang, Jiajun Song, Yuzhe Li, Linghao Zhu, Qidi Luo, Xinyu Wang, Hao Lu, Mingxin Huang, et al. Ocrbench v2: An improved benchmark for evaluating large multimodal models on visual text localization and reasoning. *arXiv preprint arXiv:2501.00321*, 2024.

- Hongcheng Gao, Jiashu Qu, Jingyi Tang, Baolong Bi, Yue Liu, Hongyu Chen, Li Liang, Li Su, and Qingming Huang. Exploring hallucination of large multimodal models in video understanding: Benchmark, analysis and mitigation. *arXiv preprint arXiv:2503.19622*, 2025. doi: 10.48550/arXiv.2503.19622. URL <https://arxiv.org/abs/2503.19622>.
- Dong Guo, Faming Wu, Feida Zhu, Fuxing Leng, Guang Shi, Haobin Chen, Haoqi Fan, Jian Wang, Jianyu Jiang, Jiawei Wang, et al. Seed1. 5-v1 technical report. *arXiv preprint arXiv:2505.07062*, 2025.
- Yixu Huang, Bo Li, Na Li, Zhe Wang, Kaijie Chen, Haonan Ge, Qingyi Si, Yuanzhe Shen, Ruihan Yang, Guangjing Wang, and Hongcheng Guo. Gui agents for continual game generation. *arXiv preprint arXiv:2605.28258*, 2026. doi: 10.48550/arXiv.2605.28258.
- Li Li, Jiashu Qu, Linxin Song, Yuxiao Zhou, Yuehan Qin, Tiankai Yang, and Yue Zhao. Treble counterfactual VLMs: A causal approach to hallucination. In Christos Christodoulopoulos, Tanmoy Chakraborty, Carolyn Rose, and Violet Peng, editors, *Findings of the Association for Computational Linguistics: EMNLP 2025*, pages 18423–18434, Suzhou, China, November 2025. Association for Computational Linguistics. ISBN 979-8-89176-335-7. doi: 10.18653/v1/2025.findings-emnlp.1000. URL <https://aclanthology.org/2025.findings-emnlp.1000/>.
- Yuliang Liu, Jiaxin Zhang, Dezhi Peng, Mingxin Huang, Xinyu Wang, Jingqun Tang, Can Huang, Dahua Lin, Chunhua Shen, Xiang Bai, et al. Spts v2: single-point scene text spotting. *IEEE Transactions on Pattern Analysis and Machine Intelligence*, 2023.
- Jinghui Lu, Haiyang Yu, Yanjie Wang, Yongjie Ye, Jingqun Tang, Ziwei Yang, Binghong Wu, Qi Liu, Hao Feng, Han Wang, et al. A bounding box is worth one token: Interleaving layout and text in a large language model for document understanding. *arXiv preprint arXiv:2407.01976*, 2024.
- Jinghui Lu, Haiyang Yu, Siliang Xu, Shiwei Ran, Guozhi Tang, Siqi Wang, Bin Shan, Teng Fu, Hao Feng, Jingqun Tang, et al. Prolonged reasoning is not all you need: Certainty-based adaptive routing for efficient llm/mlm reasoning. *arXiv preprint arXiv:2505.15154*, 2025.
- Bin Shan, Xiang Fei, Wei Shi, An-Lan Wang, Guozhi Tang, Lei Liao, Jingqun Tang, Xiang Bai, and Can Huang. Mctbench: Multimodal cognition towards text-rich visual scenes benchmark. *arXiv preprint arXiv:2410.11538*, 2024.
- Shanghai AI Lab, Yicheng Bao, Guanxu Chen, Mingkang Chen, Yunhao Chen, Chiyu Chen, Lingjie Chen, Sirui Chen, Xinquan Chen, Jie Cheng, Yu Cheng, Dengke Deng, Yizhuo Ding, Dan Ding, Xiaoshan Ding, Yi Ding, Zhichen Dong, Lingxiao Du, Yuyu Fan, Xinchun Feng, Yanwei Fu, Yuxuan Gao, Ruijun Ge, Tianle Gu, Lujun Gui, Jiakuan Guo, Qianxi He, Yuenan Hou, Xuhao Hu, Hong Huang, Kaichen Huang, Shiyang Huang, Yuxian Jiang, Shanzhe Lei, Jie Li, Lijun Li, Hao Li, Juncheng Li, Xiangtian Li, Yafu Li, Lingyu Li, Xueyan Li, Haotian Liang, Dongrui Liu, Qihua Liu, Zhixuan Liu, Bangwei Liu, Huacan Liu, Yuexiao Liu, Zongkai Liu, Chaochao Lu, Yudong Lu, Xiaoya Lu, Zhenghao Lu, et al. Safework-r1: Coevolving safety and intelligence under the AI-45° law. *arXiv preprint arXiv:2507.18576*, 2025. doi: 10.48550/arXiv.2507.18576. URL <https://arxiv.org/abs/2507.18576>.
- Wenhao Sun, Xue-Mei Dong, Benlei Cui, and Jingqun Tang. Attentive eraser: Unleashing diffusion model’s object removal potential via self-attention redirection guidance. In *Proceedings of the AAAI Conference on Artificial Intelligence*, volume 39, pages 20734–20742, 2025.
- Jingqun Tang, Wenming Qian, Luchuan Song, Xiena Dong, Lan Li, and Xiang Bai. Optimal boxes: boosting end-to-end scene text recognition by adjusting annotated bounding boxes via reinforcement learning. In *European Conference on Computer Vision*, pages 233–248. Springer, 2022a.
- Jingqun Tang, Su Qiao, Benlei Cui, Yuhang Ma, Sheng Zhang, and Dimitrios Kanoulas. You can even annotate text with voice: Transcription-only-supervised text spotting. In *Proceedings of the 30th ACM International Conference on Multimedia*, MM ’22, pages 4154–4163, New York, NY, USA, 2022b. Association for Computing Machinery. ISBN 9781450392037. doi: 10.1145/3503161.3547787. URL <https://doi.org/10.1145/3503161.3547787>.

- Jingqun Tang, Wenqing Zhang, Hongye Liu, MingKun Yang, Bo Jiang, Guanglong Hu, and Xiang Bai. Few could be better than all: Feature sampling and grouping for scene text detection. In *Proceedings of the IEEE/CVF Conference on Computer Vision and Pattern Recognition*, pages 4563–4572, 2022c.
- Jingqun Tang, Weidong Du, Bin Wang, Wenyang Zhou, Shuqi Mei, Tao Xue, Xing Xu, and Hai Zhang. Character recognition competition for street view shop signs. *National Science Review*, 10(6):nwad141, 2023.
- Jingqun Tang, Chunhui Lin, Zhen Zhao, Shu Wei, Binghong Wu, Qi Liu, Hao Feng, Yang Li, Siqi Wang, Lei Liao, et al. Textsquare: Scaling up text-centric visual instruction tuning. *arXiv preprint arXiv:2404.12803*, 2024a.
- Jingqun Tang, Qi Liu, Yongjie Ye, Jinghui Lu, Shu Wei, Chunhui Lin, Wanqing Li, Mohamad Fitri Faiz Bin Mahmood, Hao Feng, Zhen Zhao, et al. Mtvqa: Benchmarking multilingual text-centric visual question answering. *arXiv preprint arXiv:2405.11985*, 2024b.
- An-Lan Wang, Bin Shan, Wei Shi, Kun-Yu Lin, Xiang Fei, Guozhi Tang, Lei Liao, Jingqun Tang, Can Huang, and Wei-Shi Zheng. Pargo: Bridging vision-language with partial and global views. In *Proceedings of the AAAI Conference on Artificial Intelligence*, volume 39, pages 7491–7499, 2025a.
- An-Lan Wang, Jingqun Tang, Liao Lei, Hao Feng, Qi Liu, Xiang Fei, Jinghui Lu, Han Wang, Weiwei Liu, Hao Liu, et al. Wilddoc: How far are we from achieving comprehensive and robust document understanding in the wild? *arXiv preprint arXiv:2505.11015*, 2025b.
- Han Wang, Yongjie Ye, Bingru Li, Yuxiang Nie, Jinghui Lu, Jingqun Tang, Yanjie Wang, and Can Huang. Vision as lora. *arXiv preprint arXiv:2503.20680*, 2025c.
- Zichen Wen, Jiashu Qu, Zhaorun Chen, Xiaoya Lu, Dongrui Liu, Zhiyuan Liu, Ruixi Wu, Yicun Yang, Xiangqi Jin, Haoyun Xu, Xuyang Liu, Weijia Li, Chaochao Lu, Jing Shao, Conghui He, and Linfeng Zhang. The devil behind the mask: An emergent safety vulnerability of diffusion llms. In *The Fourteenth International Conference on Learning Representations*, 2026. URL <https://openreview.net/forum?id=rIPeatvPy3>.
- Mingjie You, Kaijie Chen, and Dawei Cheng. Drdgrl: Dual-relational dynamic graph representation learning for delay-sensitive stock trend prediction. In *International Conference on Database Systems for Advanced Applications*, pages 35–50. Springer, 2026.
- Haobo Zhang, Xutao Mao, Guangyuan Dong, Ziwei Li, Xuanbo Su, Kaijie Chen, Jing Yang, and Zheng Lin. Memmark: State-evolution attribution watermarking for agent long-term memory systems. *arXiv preprint arXiv:2605.25002*, 2026.
- Qinjian Zhao, Zhihao Dou, Dinggen Zhang, Xiangyu Li, Chaoda Song, Zhongwei Wan, Xinpeng Li, Yanyan Zhang, Kaijie Chen, Qingtao Pan, et al. Stride: Strategic trajectory reasoning via discriminative estimation for verifiable reinforcement learning. *arXiv preprint arXiv:2606.15866*, 2026.
- Weichao Zhao, Hao Feng, Qi Liu, Jingqun Tang, Binghong Wu, Lei Liao, Shu Wei, Yongjie Ye, Hao Liu, Wengang Zhou, et al. Tabpedia: Towards comprehensive visual table understanding with concept synergy. *Advances in Neural Information Processing Systems*, 37:7185–7212, 2025.
- Zhen Zhao, Jingqun Tang, Chunhui Lin, Binghong Wu, Can Huang, Hao Liu, Xin Tan, Zhizhong Zhang, and Yuan Xie. Multi-modal in-context learning makes an ego-evolving scene text recognizer. In *Proceedings of the IEEE/CVF Conference on Computer Vision and Pattern Recognition*, pages 15567–15576, 2024a.
- Zhen Zhao, Jingqun Tang, Binghong Wu, Chunhui Lin, Shu Wei, Hao Liu, Xin Tan, Zhizhong Zhang, Can Huang, and Yuan Xie. Harmonizing visual text comprehension and generation. *arXiv preprint arXiv:2407.16364*, 2024b.